Laser Ignition of HTPB Fuel in Oxidizing Conditions

Felix A. Rodriguez*, Christian A. Landry, James C. Thomas, and Eric L. Petersen
J. Mike Walker Mechanical Engineering Department, Texas A&M University
College Station, TX, USA

1 Introduction

Solid-fuel ramjets (SFRJs) have high potential for use in hypersonic systems for many reasons, including their simplicity and potentially high specific impulse (I_{sp}) [1]. Desirable traits for the solid fuel in SFRJ applications are ease of ignition, high theoretical performance, and good strength characteristics [2]. The steady-state fuel regression rate is directly dependent on the air mass flow rate which is required to sustain combustion. SFRJ systems are unable to operate at stagnant conditions and need to be launched at appropriate speeds before operation, so solid rocket boosters are used for the beginning of the flight until the speed is optimal for the ramjet to operate.

In most practical cases, the flammability limits of a SFRJ fuel grain are tied to the geometry of the combustor, which defines the bulk internal flow velocity and the length of the recirculation zone. It has been shown that for a given fuel grain, the ratio of the internal-to-inlet areas (A_p/A_i) or height of the step (H) and the ratio of the internal-to-nozzle throat areas (A_p/A_t) set the flammability limits in terms of flame stability [3-4]. The dependence on these area ratios is logical because the step height impacts the size of the recirculation zone, and the A_p/A_t ratio determines the internal flow velocity. Furthermore, flammability limits tend to widen with increases in both area ratios.

However, the flame characteristics in terms of ignition, burning rate, and efficiency can be modified independent of the combustor geometry by modifying the solid fuel composition via a combination of primary ingredients and additives [2,5]. Wider flammability limits due to grain composition can allow for a smaller A_p/A_i ratio and hence a higher packing of fuel, while still maintaining a stable flame.

Liquid or solid fuels can be used for ramjet propulsion systems. Solid fuels have a higher energy density than liquid fuels which can be increased further with the addition of metal particles. Interest in SFRJ propulsion systems is greater because of the higher potential of energy densities in solid fuels. The types of fuels used are generally hydrocarbons, such as hydroxyl terminated polybutadiene (HTPB). Solid-fuel ramjets can offer specific impulses that are 200-300% higher than a solid rocket motor [2,6]. A fuel grain based on an HTPB binder with aluminum additives promises high performance and reliable strength, and is therefore a preferred fuel combination for SFRJs.

Laser ignition of metal additives, solid fuels, and solid propellants have been investigated for propellant, SFRJ, and hybrid rocket applications, and some representative examples are provided here to illustrate typical findings in the literature. Song et al. [7] investigated the effects of micro- and nano-sized boron powders at different pressures and O_2/N_2 compositions. A 200-W CO_2 laser was utilized to achieve

Correspondence to: FRod1214@tamu.edu

ignition of pressed, rectangular (7 × 7 × 2 mm) samples. Pressure and oxygen concentration were reported to have a significant effect on ignition and combustion characteristics. Nano-boron exhibited a decreased ignition delay time in comparison to micro-boron. In addition, high-speed video showed chaotic burning characteristics when the oxygen concentration was increased to 100%.

Sandall et al. [8] investigated ignition of boron- and magnesium-loaded HTPB fuel grains in a gaseous crossflow. A Coherent DIAMOND E-400 CO_2 laser was used to achieve ignition of cylindrical fuel samples (Ø6.35 × 8 mm). Several mixtures of air, oxygen, and nitrogen were tested, and 10 L/min of air and 10 L/min of oxygen were found to provide the best ignition and combustion characteristics. Magnesium was found to positively affect the burning of boron-loaded HTPB fuel grains, as long as the loading percentage was optimal (10 wt%). The optimal loading allowed for smaller fuel fragments to be ejected into the crossflow allowing enough resonance time to burn.

Li et al. [9] investigated laser ignition and combustion characteristics of nitrate ester plasticized polyether (NEPE) propellants. A 300-W CO_2 laser was used for ignition of cylindrical (Ø4 × 5 mm) samples in an inert atmosphere. Li et al. [9] varied the initial pressure and sample temperature and found that the ignition delay time (t_ign) decreased with increasing gas pressure or sample temperature. Initial temperature of the sample played a smaller role as laser power flux was increased. Li et al. [10] investigated aluminum- and magnesium-loaded AP/HTPB solid propellants in a combustion chamber with optical access. Ignition of cylindrical samples (Ø4 × 7 mm) was achieved with a 300-W CO_2 laser. Pressure and oxygen concentration were varied in the study. The study reported that as pressure and oxygen concentration increased, the burning rate increased and the ignition delay time decreased.

Laser ignition of metals, fuels, and propellants is documented within the literature. Ignition and steady-state combustion characteristics of these materials vary based on their composition, surrounding atmosphere composition (i.e., oxygen concentration), and operating conditions (e.g., pressure and temperature). Laser heating also provides a known, constant heat flux that approaches the heat flux conditions that a solid fuel will see in a practical motor environment [2]. The ignition and laser-driven combustion characteristics of fuels for SFRJ applications, such as HTPB, have not been thoroughly investigated, and the current study aims to address this knowledge gap. In the current study, an existing constant-volume strand burner was used to simulate the combustion conditions in a SFRJ. Fuel strands (HTPB) were remotely ignited in an oxidizer atmosphere (air) with a CO_2 laser over a range of power fluxes at a representative pressure condition. The following section details the experimental methodology, followed by results and discussion, and conclusions and recommendations sections.

2 Experimental Methods

The HTPB and isophorone diisocyanate (IPDI) were acquired from Cray Valley and Millipore Sigma, respectively. Samples investigated here were manufactured using a 10.44:1 mass cure ratio of HTPB to IPDI (–NCO/–OH=1). The materials were mixed for twenty minutes in a beaker with intermittent heating. The mixture was subsequently vacuumed for roughly one hour to remove all entrained air bubbles. The mixture was then cast into ¼″-diameter Teflon tubing and cured at 63 ℃ for seven days. Sample mass and length were measured with a scale (resolution of 0.01 g) and calipers (resolution of 0.01 mm), respectively. Experimentally measured densities ranged from 92-105% the theoretical maximum density (930 kg/m3) which is reasonable considering the measurement error (~±5%).

A constant-volume combustion chamber, referred to herein as a strand burner was used to conduct laser ignition experiments of HTPB (Ø6.35 × ~4 mm) in a dry air atmosphere at an initial pressure of 8.96 ± 0.34 bar (130 ± 5 psia). In-line pressure transducers (OmegaDyne PX02C1-7.5KG) tracked the pressure rise during combustion. There are three optically accessible windows on the sides of the strand burner that allow for various diagnostics including a high-speed video camera (Photron FASTCAM SA3 120K), a photodiode (New Focus 2031) used to collect light emission data, and a visible/near-infrared spectrometer (Ocean Optics USB2000). High-speed video and light emission data were collected for all

experiments conducted herein. A ZnSe window is located on the top of the strand burner (directly above the propellant stand) and allows for CO_2 laser ignition. A Firestar series ti100 CO_2 laser with a wavelength of 10.6 μm was used. A schematic of the experimental setup is shown in Fig. 1, and further details are provided by Krietz et al. [11] and Demko et al. [12-13].

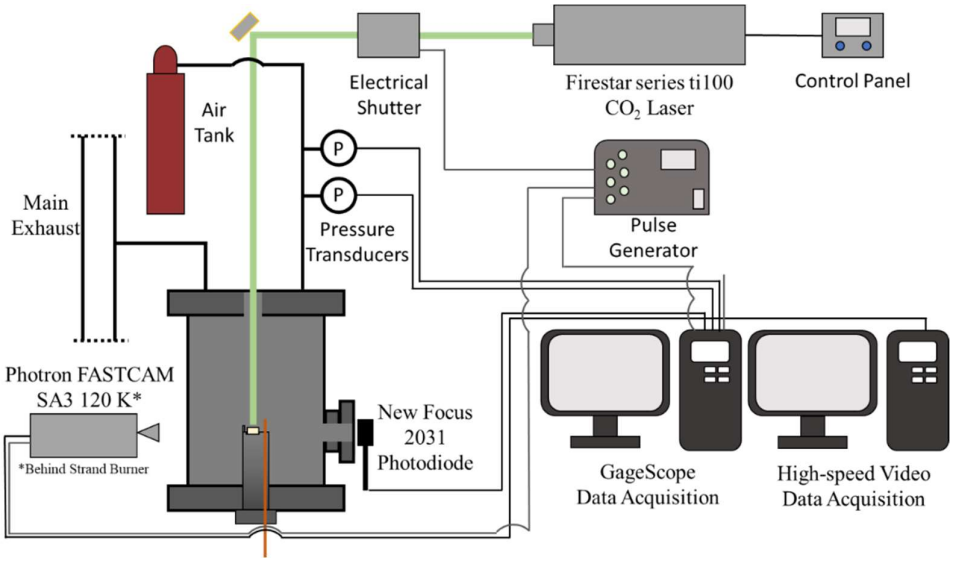

Figure 1: Schematic of the constant-volume strand burner used for laser ignition experiments. Key diagnostics include pressure transducers, high-speed video, and a photodiode.

The CO_2 laser beam passes through a electrical shutter, is reflected by a gold mirror (NB1-L01), passes through a ZnSe window, and impinges on the propellant surface, as shown in Fig. 1. A mechanical iris was used to align the beam so that it impinged in the middle of the fuel surface. The transmitted laser power was calibrated prior to conducting any ignition delay time experiments. The laser input power is controlled with pulse width modulation (PWM). A laser power meter (Cloudray 200 W Handheld CO_2 Laser Power Meter) was used to measure the transmitted power that reaches the fuel sample surface to the input power (% PWM). The input power was varied over the entire operating range (3-95% PWM) and was used to build a calibrated, transmitted power curve. The beam diameter (3.1 ± 0.5 mm), which is smaller than the fuel sample diameter, was measured with the mechanical iris coupled with a thermal alignment card and separately with a burnable stock paper card. Multiple transmitted power measurements were taken at several power conditions to determine the deviation in output readings, and they were all within the uncertainty of the power meter (0.1 W). The uncertainty between the correlation equation and the data collected was ±1 W. The maximum transmitter power achieved (~60 W) is significantly lower than the maximum possible power (100 W) due to reflectance losses on the gold mirror and transmittance losses through the ZnSe window. However, the achieved transmitted power is sufficient for the current study.

Ballistic testing was conducted remotely. Prior to an experiment, the strand burner was slowly filled with air to the appropriate pressure, the laser power was set by a percentage of pulse width modulation (ex. 55% PWM), and the laser was turned on. A pulse generator (BNC Model 575 Pulse/Delay Generator) sent a signal to the data acquisition system (GageScope), the electrical shutter, and the high-speed camera to initiate the experiment. The electrical shutter was used to finely control laser exposure. The authors' laboratory previously designed and characterized the same shutter system, and it was measured to have a delay of 29 ms before the shutter was fully open [13]. A representative experimental data trace is shown in Fig. 2. The pressure trace, shutter signal, and average pressure are represented by black, red, and green lines, respectively. The blue points are light emission data. Letter labels have been placed on Fig. 2 to highlight key details. The start of a test is shown by the shutter signal increasing (Fig. 2, point

A). The fuel sample ignites some time after the shutter is opened, which causes a deviation from the baseline light emission signal (Fig. 2, point B). The light emission signal subsequently saturates at 2.0 V (Fig. 2, point C). The pulse generator is triggered to send an additional signal, closing the shutter once the data acquisition is complete (Fig. 2, point D).

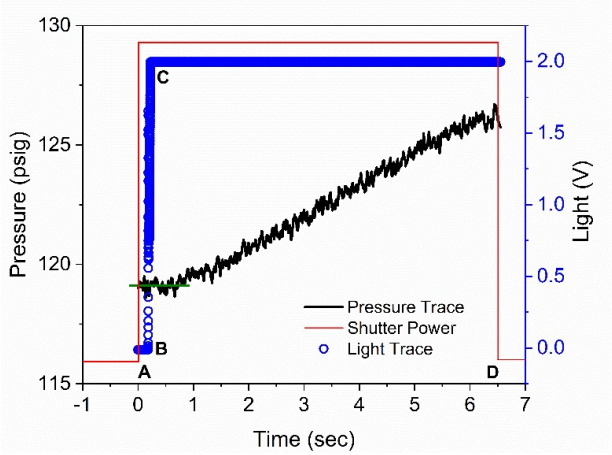

Figure 2: An example data trace with pressure (black), shutter signal (red), light emission data (blue), and average pressure line (green). Letter labels are placed to highlight key details.

Four separate methods to determine the ignition delay time based on light emission data or high-speed video were evaluated herein. All ignition delay time data were reduced by 29 ms to account for the electrical shutter opening. The ignition delay times based on the light emission trace were measured from the shutter opening time to the first point where the light emission trace deviated from the baseline value (Fig. 2, point B) or to the first point where the light emission trace was saturated (Fig. 2, point C). Example snapshots from a representative high-speed video are shown in Fig. 3. The left and right images depict condensed-phase luminescence and vapor-phase ignition, respectively. Condensed-phase luminescence occurred due to fuel fragments on the surface from the filling process and would glow without any flame propagation. Vapor-phase combustion would emit light and propagate upward in a mushroom cloud shape. The ignition delay times based on high-speed video analysis were measured from the shutter opening time to first frame where condensed-phase luminescence or vapor-phase ignition were observed. In general, the frame where condensed-phase luminescence and vapor-phase ignition were observed coincided or the vapor-phase ignition took place soon after (< 2 ms) condensed-phase luminescence was observed. However, persistent condensed-phase luminescence without rapid vapor-phase ignition was observed in several experiments. This disparity was attributed to small, detached fuel fragments leftover from the fuel preparation and cutting process being heated on the surface of the bulk fuel sample.

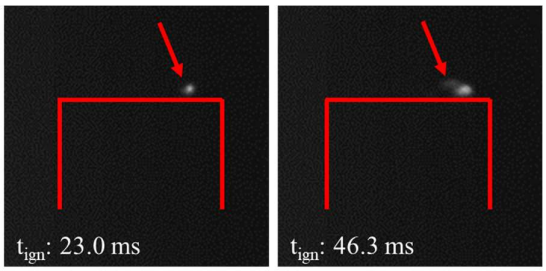

Figure 3: Example high-speed video snapshots illustrating (left) condensed luminescence and (right) vapor-phase ignition during a single laser ignition experiment. Red lines denote the propellant surface.

3 Results and Discussion

Ignition delay time data for HTPB in air at 8.96 ± 0.34 bar (130 ± 5) psia collected by all four methods previously discussed are shown in Fig. 4 (left). In general, the ignition delay time decreased as the laser power flux increased, as expected. The high-speed video vapor-phase ignition measurement approach for ignition delay time proved to be the most consistent and reliable metric for this experiment. In addition, vapor-phase ignition is the best analog for SFRJ ignition in realistic applications. Ignition delay time measurements based on the light emission trace's first deviation and saturation were well correlated with condensed-phase luminescence and vapor-phase ignition in the high-speed videos, so saturation of the light emission is considered the second-best approach evaluated herein.

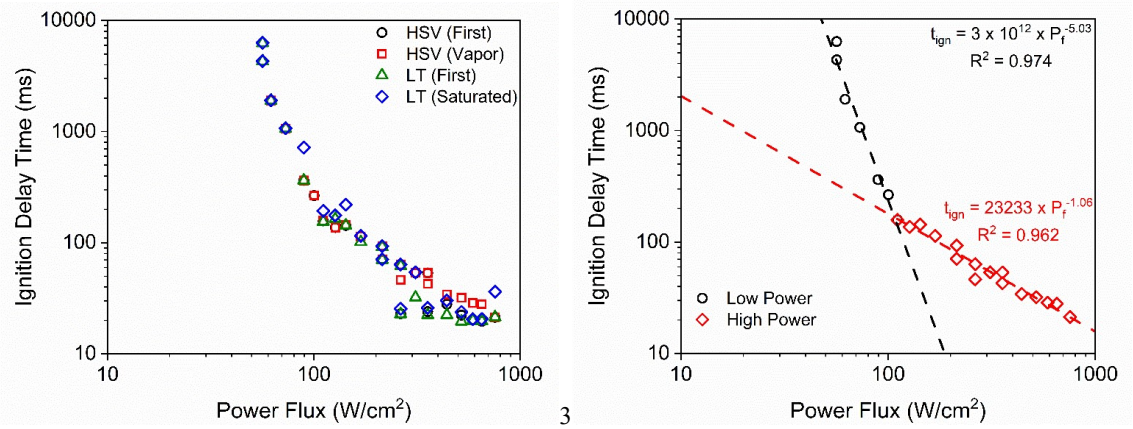

Figure 4: (left) Ignition delay time data at 8.96 ± 0.34 bar (130 ± 5 psia) for all four data analysis methods based on the light emission trace and high-speed video. (right) Vapor-phase ignition delay times from high-speed video data for HTPB fuel in air at 8.96 ± 0.34 bar (130 ± 5 psia).

Figure 4 (right) shows the ignition delay time data determined from vapor-phase ignition in high-speed videos. Two separate regions with distinctly different trends were observed in the dataset. The negative ignition delay time data slope is significantly greater in the low-power region (< 110 W/cm^2) in comparison the high-power region. Power law correlations fit the data well in both regions. The change in slope may be related to heat losses playing a more prominent role in the lower-power region where longer time scales are required for ignition, but further investigation is required to confirm this hypothesis.

4 Conclusions and Recommendations

The laser ignition and combustion characteristics of HTPB were probed in the current study. The laser experimental setup was calibrated and subsequently used to ignite small samples of HTPB in air at a constant air pressure condition, 8.96 ± 0.34 bar (130 ± 5 psia), and variable power fluxes. The high-speed video and light emission data diagnostics were successful at discerning condensed-phase luminescence and vapor-phase ignition phases observed in these experiments. Four methods of determining an ignition delay time were detailed. Measurement based on the first light associated with vapor phase combustion in high-speed video analysis exhibited the most consistent and relevant ignition delay time results.

The laser power flux was varied over a large range (55-755 W/cm^2), and the ignition delay time of HTPB in air was observed to decrease with increasing power flux. Two different regions were observed in the ignition delay time data. A significantly steeper slope in the ignition delay time curve was observed in the low-power region (< 110 W/cm^2) than in comparison to the high-power region. The

disparate slopes were theorized to be influenced by heat transfer effects, potentially from the sample and into the sample holder.

The laser ignition experimental capability developed in the current study for solid-fuel systems provides the opportunity for further fundamental and applied investigations in this technical area. Future work may include evaluation of the effects of bath gas pressure, temperature, and composition (O_2/N_2 ratio) on the ignition delay time of HTPB-based fuels. These fuels may also include metallic additives which can boost the energy density of SFRJ systems. In addition, the steady-state independent and laser-driven regression rates of these fuels in various oxidizing environments could be studied to better understand the underlying combustion phenomena and relative significance of heat transfer modes (radiation, conduction, and convection).

References

[1] Rathi NJ, Ramakrishna PA. (2017). Attaining Hypersonic Flight with Aluminum-Based Fuel-Rich Propellant. J. Propuls. Power. 33: 1207.

[2] Hedman TD, Quigley JN, Kalman J, Washburn EB. (2017). Small-Scale Solid Ramjet Fuel Ignition Experiment. J. Propuls. Power. 33: 1315.

[3] Netzer A, Gany A. (1991). Burning and Flameholding Characteristics of a Miniature Solid Fuel Ramjet Combustor. J. Propuls. Power. 7: 357.

[4] Wooldridge RC, Netzer DW. (1991). Ignition and Flammability Characteristics of Solid Fuel Ramjets. J. Propuls. Power. 7: 846.

[5] Simone D, Bruno C. (2009). Preliminary Investigation on Lithium Hydride as Fuel for Solid-Fueled Scramjet Engines. J. Propuls. Power. 25: 875.

[6] Krishnan S, George P. (1998). Solid Fuel Ramjet Combustor Design. Prog. Aerosp. Sci. 34: 219.

[7] Song Q, Cao W, Wei X, Liu J, Yuan J, Li X, Guo X, Gao D. (2021). Laser Ignition and Combustion Characteristics of Micro- and Nano-sized Boron Under Different Atmospheres and Pressures. Combust. Flame. 120: 107268.

[8] Sandall ET, Kalman J, Quigley JN, Munro S, Hedman TD. (2017). A Study of Solid Ramjet Fuel Containing Boron-Magnesium Mixtures. Propuls. Power. Res. 6: 243.

[9] Li L, Chen X, Zhou C, Zhu M, Musa O. (2017). Experimental Investigation on Laser Ignition and Combustion Characteristics of NEPE Propellant. Propellants Explos. Pyrotechnics. 42: 1095.

[10] Li L, Chen X, Musa O, Zhou C, Zhu M. (2018). The Effect of Pressure and Oxygen Concentration on the Ignition and Combustion of Aluminum-Magnesium Fuel-Rich Propellants. Aerosp. Sci. Technol. 76: 394.

[11] Kreitz KR, Petersen EL, Reid DL, Seal S. (2011). Relative Dispersion of Catalytic Nanoparticle Additives and AP Particles in Composite Solid Propellant and the Effect on Burning Rate. 49th AIAA Aerospace Sciences Meeting.

[12] Demko AR, Allen TW, Dillier C, Sammet T, Reid DL, Seal S, Petersen EL. (2018). Temperature Sensitivity of Composite Propellants Containing Novel Nano-Additive Catalysts. J. Propuls. Power. 34: 795.

[13] Demko A. (2017). Advancements in Composite Solid Propellant Testing and Evaluation for Formulations Containing Novel Nano-Additives. Ph.D. Dissertation. Texas A&M University.